Space-Domain Decoupling of LSE and LSM Fields In Generalized Planar Guiding Structures

ABBAS SAYED OMAR AND KLAUS SCHÜNEMANN, MEMBER IEEE

Abstract—**LSE and LSM fields in generalized planar guiding structures are shown to be coupled only by means of the edge condition, which can be fulfilled as the final step in the analysis. This is utilized by applying the singular integral equation technique to finlines. Modes up to the thirtieth are thus easily and quickly computed.**

I. Introduction

THE HYBRID NATURE of the electromagnetic field in generalized planar guiding structures (which consist of an arbitrary number of dielectric layers with metal strips being arbitrarily deposited at the interfaces) is the main source of complexity in the analysis. Knowing the physical reasons for the coupling between the two parts of the field would allow one to treat these fields independently, up to the point where the coupling enters the analysis. In this respect, both TE and TM fields must be coupled from the beginning because the air–dielectric or the dielectric–dielectric interface conditions cannot be satisfied otherwise. On the other hand, these interface conditions are independently fulfilled by the LSE and LSM field parts [1], whereas the fields are just coupled in order to satisfy the edge condition. This will be derived in the following. (The edge condition is, e.g., defined in [2].) The LSE and LSM field parts can then independently be treated in the analysis up to the point at which the edge condition has to be satisfied. This can, however, be done in a final step, thus greatly simplifying the analysis.

This kind of decoupling between the LSE and LSM field parts in some planar guiding structures has already been utilized in the spectral domain, where the spectral representations of the field components are related by algebraic equations [3]–[9]. It has been shown to be very effective there in reducing the complexity of the analysis. In [3]–[6], the spectral representations of the hybrid field have been decoupled into LSE and LSM parts and treated independently by using the equivalent transmission-line concept. They have been coupled in the final step of the analysis without giving a special reason. In [7]–[9], LSE and LSM decoupling has also been utilized. Both field parts have independently been treated by the Wiener–Hopf technique. Coupling has been introduced in the final step in order to eliminate singularities which occurred in the course of the back-transformation of the LSE and LSM fields into the hybrid field. A physical reason for the coupling has not been given.

A possible decoupling between LSE and LSM fields in the space domain is much more important than in the spectral domain because the field components are now related by integral instead of algebraic equations. Dealing with uncoupled integral equations facilitates the analysis to a great extent, in particular if structures with more than one dielectric layer are to be treated.

Manuscript received April 26, 1984. This work was supported by Deutsche Forschungsgemeinschaft.

The authors are with the Technische Universität Hamburg–Harburg, Arbeitsbereich Hochfrequenztechnik, Postfach 90 14 03, D-2100 Hamburg 90, West Germany.

II. Basic Formulation

The generalized planar guiding structure sketched in Fig. 1 shows an arbitrary number of air–dielectric and/or dielectric–dielectric interfaces which are in parallel to the direction of wave propagation (taken as z-direction here). Infinitely thin metal strips are assumed to be deposited at the interface in the $(x = 0)$-plane, although the analysis can easily be extended to the case that there are strips at more than one interface. LSE and LSM fields independently satisfy all the interface conditions at the strip-free interfaces [1]. Hence, it suffices to consider just the interface conditions in the $(x = 0)$-plane.

A. LSE Field

For perfectly conducting strips, the LSE field in regions 1 and 2 can be expressed in terms of scalar potentials ψ_1^h and ψ_2^h satisfying the Helmholtz equation

$$\frac{\partial^2 \psi_i^h}{\partial x^2} + \frac{\partial^2 \psi_i^h}{\partial y^2} + \left(\kappa_i k_0^2 - \beta^2\right) = 0, \qquad i = 1,2. \tag{1}$$

Here, wave propagation has been described by $\exp(-j\beta z)$, $k_0^2 = \omega^2 \mu_0 \epsilon_0$, and κ_i is the dielectric constant of region i. The tangential field components at the interface are calculated from

$$E_y^{(i)} = -\omega\mu_0 \beta \psi_i^h, \qquad H_y^{(i)} = \frac{\partial^2 \psi_i^h}{\partial x \partial y}$$

$$E_z^{(i)} = j\omega\mu_0 \frac{\partial \psi_i^h}{\partial y}, \qquad H_z^{(i)} = -j\beta \frac{\partial \psi_i^h}{\partial x}. \tag{2}$$

0018-9480/84/1200-1626$01.00

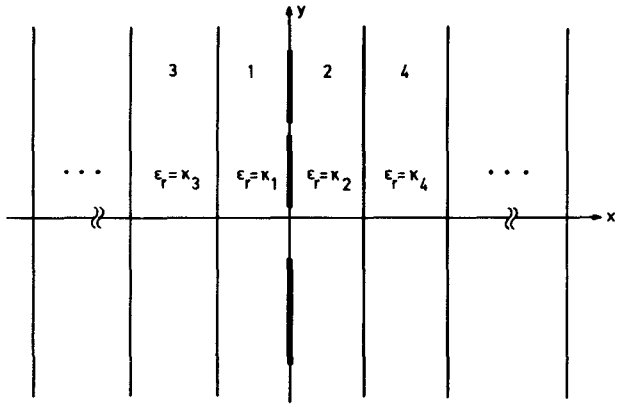

Fig. 1. Generalized planar guiding structure.

The interface conditions read

$$E_y^{(1)} = E_y^{(2)} = E_y, \qquad E_z^{(1)} = E_z^{(2)} = E_z$$
$$H_z^{(1)} - H_z^{(2)} = J_r, \qquad H_y^{(2)} - H_y^{(1)} = J_z, \qquad \text{at } x = 0. \tag{3}$$

E_y, E_z are the tangential electric-field components, and J_y, J_z are surface current density components at $x = 0$.

It is proven from (2) and (3) that

$$E_z \sim \frac{dE_y}{dy}, \qquad J_z \sim \frac{dJ_y}{dy}. \tag{4}$$

Hence, the LSE field is completely characterized by the y-components of the tangential electric field and of the surface current density at the interface. Moreover, it can also be shown from (2) and (3) that both the tangential electric field $\boldsymbol{E}_t = E_y \boldsymbol{n}_y + E_z \boldsymbol{n}_z$ and the surface current density $\boldsymbol{J}_s = J_y \boldsymbol{n}_y + J_z \boldsymbol{n}_z$ are solenoidal, i.e.,

$$\nabla_t \boldsymbol{E}_t = 0, \qquad \nabla_t \boldsymbol{J}_s = 0. \tag{5}$$

$\nabla_t \triangleq (\partial/\partial y)\boldsymbol{n}_y + (\partial/\partial z)\boldsymbol{n}_z$ means two-dimensional del-operator in the y–z-plane, $\boldsymbol{n}_y$ and $\boldsymbol{n}_z$ are unit vectors in y- and z-direction, respectively.

B. LSM Field

The LSM field is similarly expressed by scalar potentials ψ_1^e and ψ_2^e satisfying (1) with superscript 'h' replaced by 'e'. The tangential field components can be derived from

$$E_y^{(i)} = \frac{1}{\epsilon_r}\frac{\partial^2 \psi_i^e}{\partial x \partial y}, \qquad H_y^{(i)} = \omega \epsilon_0 \beta \psi_i^e$$
$$E_z^{(i)} = \frac{-j\beta}{\epsilon_r}\frac{\partial \psi_i^e}{\partial x}, \qquad H_z^{(i)} = -j\omega\epsilon_0 \frac{\partial \psi_i^e}{\partial y} \tag{6}$$

with interface conditions given by (3). It can now be derived from (6) and (3) that

$$E_y \sim \frac{dE_z}{dy}, \qquad J_y \sim \frac{dJ_z}{dy} \tag{7}$$

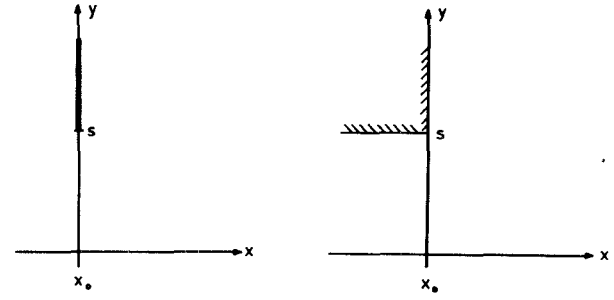

Fig. 2. Coordinates of (a) the 0° edge and (b) the 90° edge.

so that the LSM field is completely characterized by the z-components of $\boldsymbol{E}_t$ and $\boldsymbol{J}_s$. Furthermore, both $\boldsymbol{E}_t$ and $\boldsymbol{J}_s$ show zero curl

$$\nabla_t \times \boldsymbol{E}_t = 0, \qquad \nabla_t \times \boldsymbol{J}_s = 0. \tag{8}$$

C. Edge Condition

It will now be shown that the edge condition [2] establishes a coupling between the LSE and LSM field parts. It states that both E_y and J_z are singular at the edges of the metal strips, whereas E_z and J_y behave regularly, viz., they are vanishing here. For the LSE field, the z-components E_z^h and J_z^h are both proportional to the y-derivative of the y-components E_y^h and J_y^h (4). E_z^h cannot behave regularly at the edges if E_y^h is singular here, because the derivative of a function shows a stronger singularity than the function itself. A similar conclusion can be drawn for J_y^e of the LSM field. The edge condition can only be satisfied by a linear combination of LSE and LSM fields according to

$$\boldsymbol{E}_t = \boldsymbol{E}_t^e + \boldsymbol{E}_t^h, \qquad \boldsymbol{J}_s = \boldsymbol{J}_s^e + \boldsymbol{J}_s^h. \tag{9}$$

The individual components in (9) must show the following behavior at the edges:

1) E_y^h and J_z^e are regular with regular y-derivative, and
2) E_z^e and J_y^h are regular with singular y-derivative.

Hence, it can be concluded that the LSE field is responsible for the edge singularity of J_z, while the LSM field creates that of E_y.

The validity of this discussion is not restricted to the idealized case of infinitely thin strips. It can be applied equally when the finite thickness is taken into account because both the 0° edge and the 90° edge have a similar effect on the field components with respect to singularity, in both cases, E_y and J_z behave singularly, whereas E_z and J_y are regular. Referring to Fig. 2, one has at $x = x_0^+$ for $y \to s$

$$\left.\begin{aligned}(E_y,\ J_z) &\sim |y-s|^{-1/2}\\ (E_z,\ J_y) &\sim |y-s|^{+1/2}\end{aligned}\right\} \quad 0° \text{ edge}$$

$$\left.\begin{aligned}(E_y,\ J_z) &\sim |y-s|^{-1/3}\\ (E_z,\ J_y) &\sim |y-s|^{+2/3}\end{aligned}\right\} \quad 90° \text{ edge.} \tag{10}$$

A closely related problem is that of an E-plane step in a

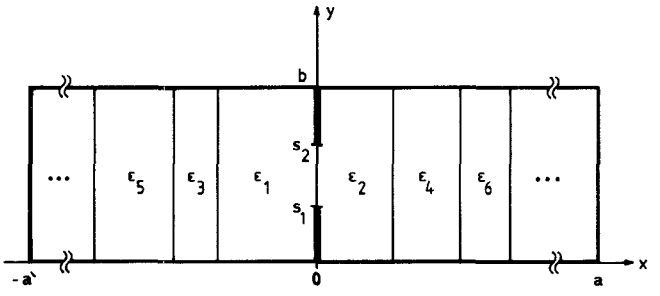

Fig. 3. Generalized unilateral finline.

rectangular waveguide which cannot support a purely TE field if it is excited by the dominant mode. The only reason for this is that the edge condition would then be violated.

III. Application to Singular Integral Equation Technique

One of the most powerful space-domain methods is the singular integral equation technique which has been used in [10]–[12] for solving a variety of waveguide problems. It has also been applied to the analysis of microstrip lines [13], [14]. Using this technique for the analysis of generalized planar structures has the same advantages as the well-known and widely used Galerkin method in the spectral domain—the small order of the matrix characterizing the problem. For the dominant and the first few high-order modes of any planar guiding structure, the Galerkin method in spectral domain is superior over all other methods because the order of the characteristic matrix may be as low as four (corresponding to two basis functions for each component of either strip current or slot electric field) for still excellent accuracy. For higher order modes up to the tenth or twentieth, which are needed in the analysis of discontinuities, two basis functions are not sufficient to approximate the real field, so that the order of the matrix must be increased considerably. In this case, the singular integral equation technique becomes preferable because a matrix of order seven is quite sufficient for achieving accurate results up to the thirtieth mode [15].

Utilizing the decoupling between LSE and LSM fields derived above, the singular integral equation technique leads to two uncoupled singular integral equations which can be solved by standard methods [11]. In a subsequent final step, the coupling is then taken into account in order to fulfill the edge condition. The procedure is illustrated here by analyzing the generalized unilateral finline structure sketched in Fig. 3. Four functions are defined at the interface $x = 0$ by

$$\frac{df_1^e}{dy} = C_1^e \nabla_t \boldsymbol{E}_t, \qquad f_2^e = C_2^e \nabla_t \boldsymbol{J}_s$$

$$f_1^h = C_1^h \boldsymbol{n}_x (\nabla_t \times \boldsymbol{E}_t), \qquad \frac{df_2^h}{dy} = C_2^h \boldsymbol{n}_x (\nabla_t \times \boldsymbol{J}_s). \quad (11)$$

$C_1^e \cdots C_2^h$ are constants, $\boldsymbol{n}_x$ means unit vector in the x-direction.

Comparing (11) with (5) and (8), it can be seen that f_1^e and f_2^e represent the LSM part of the field, while f_1^h and f_2^h represent its LSE part. For perfectly conducting walls at $y = 0$ and $y = b$, these functions can be expanded into Fourier series with two sets of unknown coefficients

$$f_1^e = \sum_{n=1}^{\infty} A_n^e \cos(n\pi y/b),$$

$$f_2^e = \sum_{n=1}^{\infty} P_n A_n^e \sin(n\pi y/b)$$

$$f_1^h = A_0^h + \sum_{n=1}^{\infty} A_n^h \cos(n\pi y/b),$$

$$f_2^h = Q_0 \frac{\pi y}{b} A_0^h + \sum_{n=1}^{\infty} Q_n A_n^h \sin(n\pi y/b). \quad (12)$$

In (12), $A_n^e(P_n)$ and $A_n^h(Q_n)$ are proportional to the Fourier expansion coefficients of the LSM and LSE fields (Green's functions), respectively.

The construction of the four functions according to (11) guarantees that 1) P_n and Q_n have unit asymptotic limits for large n, which is approached exponentially, and that 2) $f_1^e \cdots f_2^h$ show a $(|y-s|^{-1/2})$-singularity at the edges, which is the proper type of singularity for a description by the singular integral equation technique.

The boundary conditions to be imposed on these functions read

$$\frac{df_1^e}{dy} = 0 = f_1^h, \qquad \text{for } 0 \leqq y \leqq s_1,\ s_2 \leqq y \leqq b$$

$$f_2^e = 0 = \frac{df_2^h}{dy}, \qquad \text{for } s_1 \leqq y \leqq s_2. \quad (13)$$

Following standard procedures [12], the field expansion coefficients A_n^e and A_n^h can be expressed in terms of two infinite series $g^e(y)$ and $g^h(y)$ which are defined by

$$g^e(y) = \sum_{n=1}^{\infty} (1 - P_n) A_n^e \sin(n\pi y/b)$$

$$g^h(y) = \sum_{n=1}^{\infty} (1 - Q_n) A_n^h \sin(n\pi y/b). \quad (14)$$

The coefficients in (14) obviously vanish asymptotically, so that the infinite sums can be truncated behind the first few terms. Thus, the order of the characteristic matrix will be low.

As the final step, the two field parts have to be coupled. One recognizes from (11) that the vanishing of both df_1^e/dy and f_1^h on the fins (see (13)) guarantees only that E_y and E_z satisfy Laplace's equation there. Hence, one of the two components of $\boldsymbol{E}_t$ must be set to zero at the edges [16] in order to satisfy the boundary condition $\boldsymbol{E}_t = 0$ on the fins. This establishes a first coupling relation between the LSE and the LSM field. One can conclude in a similar way that the vanishing of f_2^e and df_2^h/dy guarantees only that the

TABLE I

THE PROPAGATION CONSTANTS OF THE FIRST 20 MODES IN A BILATERAL FINLINE. PARAMETERS: $a = 2b = 3.556$ mm, SUBSTRATE THICKNESS = 0.254 mm, $s_1 = 0.0$, $s_2 = 0.2$ mm, $\epsilon_r = 2.22$, AND $f = 30$ GHz.

mode no. / matrix order	1	2	3	4	5	6	7	8	9	10
5 x 5	0.665	-j0.769	-j1.672	-j1.763	-j1.889	-j2.004	-j2.467	-j2.536	-j2.731	-j3.206
7 x 7	0.658	-j0.772	-j1.672	-j1.763	-j1.889	-j2.007	-j2.467	-j2.537	-j2.732	-j3.206
9 x 9	0.656	-j0.773	-j1.672	-j1.763	-j1.889	-j2.008	-j2.467	-j2.538	-j2.732	-j3.206

mode no. / matrix order	11	12	13	14	15	16	17	18	19	20
5 x 5	-j3.262	-j3.494	-j3.596	-j3.605	-j3.687	-j3.931	-j3.961	-j4.019	-j4.114	-j4.432
7 x 7	-j3.262	-j3.494	-j3.596	-j3.605	-j3.687	-j3.931	-j3.961	-j4.019	-j4.112	-j4.432
9 x 9	-j3.262	-j3.494	-j3.596	-j3.605	-j3.687	-j3.931	-j3.961	-j4.019	-j4.112	-j4.432

TABLE II

MODE COUPLING COEFFICIENTS FOR THE FIRST 10 MODES. PARAMETERS AS IN TABLE I

i \ j	1	2	3	4	5	6	7	8	9	10
1	$+1.0$	$-j2.6\cdot10^{-3}$	$-j8.2\cdot10^{-4}$	$-j1.7\cdot10^{-3}$	$+j4.5\cdot10^{-2}$	$-j3.6\cdot10^{-3}$	$+j8.4\cdot10^{-3}$	$-j2.4\cdot10^{-3}$	$-j2.7\cdot10^{-3}$	$+j1.1\cdot10^{-2}$
2	$-j2.2\cdot10^{-3}$	$+j1.0$	$-j2.9\cdot10^{-4}$	$-j6.0\cdot10^{-4}$	$+j2.2\cdot10^{-2}$	$-j1.3\cdot10^{-3}$	$+j.36\cdot10^{-3}$	$-j8.4\cdot10^{-4}$	$-j9.8\cdot10^{-4}$	$+j4.4\cdot10^{-3}$
3	$-j3.1\cdot10^{-4}$	$-j1.3\cdot10^{-4}$	$+j1.0$	$-j8.1\cdot10^{-5}$	$+j1.4\cdot10^{-2}$	$-j1.7\cdot10^{-4}$	$+j9.6\cdot10^{-4}$	$-j1.1\cdot10^{-4}$	$-j1.3\cdot10^{-4}$	$+j9.1\cdot10^{-4}$
4	$-j6.3\cdot10^{-4}$	$-j2.6\cdot10^{-4}$	$-j7.8\cdot10^{-5}$	$+j1.0$	$+j4.2\cdot10^{-2}$	$-j3.5\cdot10^{-4}$	$-j3.5\cdot10^{-4}$	$-j2.3\cdot10^{-4}$	$-j2.7\cdot10^{-4}$	$+j1.7\cdot10^{-3}$
5	$+j1.5\cdot10^{-2}$	$+j2.8\cdot10^{-2}$	$+j1.2\cdot10^{-2}$	$+j3.9\cdot10^{-2}$	$-j1.0$	$-j8.7\cdot10^{-2}$	$+j3.3\cdot10^{-6}$	$-j1.0\cdot10^{-2}$	$-j8.5\cdot10^{-3}$	$+j7.6\cdot10^{-6}$
6	$-j1.2\cdot10^{-3}$	$-j4.8\cdot10^{-4}$	$-j4.6\cdot10^{-5}$	$-j3.0\cdot10^{-4}$	$-j8.1\cdot10^{-2}$	$+j1.0$	$+j5.5\cdot10^{-3}$	$-j4.2\cdot10^{-4}$	$-j4.9\cdot10^{-4}$	$+j3.9\cdot10^{-3}$
7	$+j2.1\cdot10^{-3}$	$+j1.1\cdot10^{-3}$	$+j6.4\cdot10^{-4}$	$+j1.3\cdot10^{-3}$	$+j3.9\cdot10^{-7}$	$+j4.4\cdot10^{-3}$	$-j1.0$	$-j1.8\cdot10^{-2}$	$-j5.4\cdot10^{-3}$	$+j5.9\cdot10^{-6}$
8	$-j6.0\cdot10^{-4}$	$-j2.5\cdot10^{-4}$	$-j7.5\cdot10^{-5}$	$-j1.6\cdot10^{-4}$	$-j7.4\cdot10^{-3}$	$-j3.3\cdot10^{-4}$	$-j1.7\cdot10^{-2}$	$+j1.0$	$-j2.5\cdot10^{-4}$	$+j3.5\cdot10^{-3}$
9	$-j6.6\cdot10^{-4}$	$-j2.8\cdot10^{-4}$	$-j8.3\cdot10^{-5}$	$-j1.7\cdot10^{-4}$	$-j5.8\cdot10^{-3}$	$-j3.6\cdot10^{-4}$	$-j4.8\cdot10^{-3}$	$-j2.4\cdot10^{-4}$	$+j1.0$	$+j5.2\cdot10^{-3}$
10	$+j2.1\cdot10^{-3}$	$+j1.0\cdot10^{-3}$	$+j4.6\cdot10^{-4}$	$+j9.1\cdot10^{-4}$	$+j8.8\cdot10^{-7}$	$+j2.4\cdot10^{-3}$	$+j2.8\cdot10^{-6}$	$+j2.8\cdot10^{-3}$	$+j4.3\cdot10^{-3}$	$-j1.0$

surface current density components satisfy Laplace's equation in the slot. In order to have $J_s = 0$ here, one of its two components must be set to zero at the edges. Thus, a second coupling relation between the partial fields is established.

It should be noted that these additional coupling relations do not over-determine the problem, because a sufficient number of unknown constants has been generated until now. The number of homogeneous linear equations always equals the number of unknowns. Propagation constants and field distributions of the various modes have to be calculated from this system.

IV. NUMERICAL RESULTS

To illustrate the fast convergence in the truncation procedure, the propagation constants of the first 20 modes of a bilateral finline have been calculated for matrix orders of five, seven, and nine. (This corresponds to truncating the infinite series' in (14) behind the second, third, and fourth terms, respectively.) The results in Table I show that orders

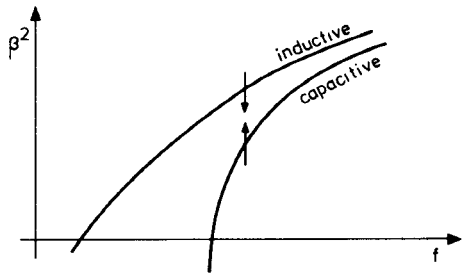

Fig. 4. Effect of slot width (increases in direction of the arrows) on the dispersion characteristic of inductive and capacitive modes.

TABLE III
THE EFFECT OF INCREASING THE SLOT WIDTH ON THE *SQUARES* OF THE PROPAGATION CONSTANTS. PARAMETERS AS IN TABLE I

modes / slotwidth	1	2	3	4	5	6	7	8	9	10	
0.4 mm	+0.430	-0.598	-2.797	-3.110	-3.567	-4.030	-6.084	-6.440	-7.466	-10.281	
1.0 mm	+0.360	-0.726	-2.801	-3.184	-3.562	-4.314	-6.067	-6.560	-7.920	-10.237	

modes / slotwidth	11	12	13	14	15	16	17	18	19	20	
0.4 mm	-10.645	-12.211	-12.932	-12.996	-13.595	-15.450	-15.689	-16.156	-16.907	-19.645	
1.0 mm	-10.976	-12.221	-12.918	-13.103	-13.869	-15.377	-15.725	-16.068	-17.419	-19.477	

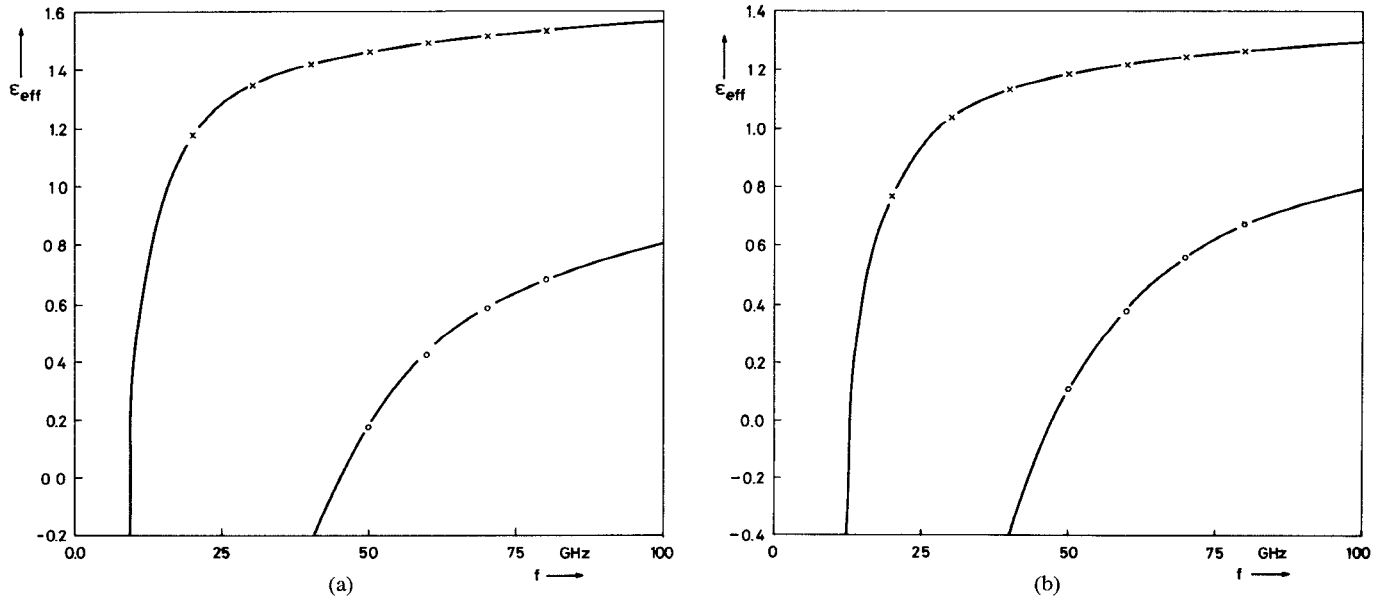

Fig. 5. Dispersion characteristics of the first two modes in a bilateral finline for slot widths (a) of 0.15 mm and (b) of 0.5 mm. ×, ○ results taken from [17], —— this method, parameters: $a = 2b = 3.556$ mm, substrate thickness 0.125 mm, $\epsilon_r = 3.0$.

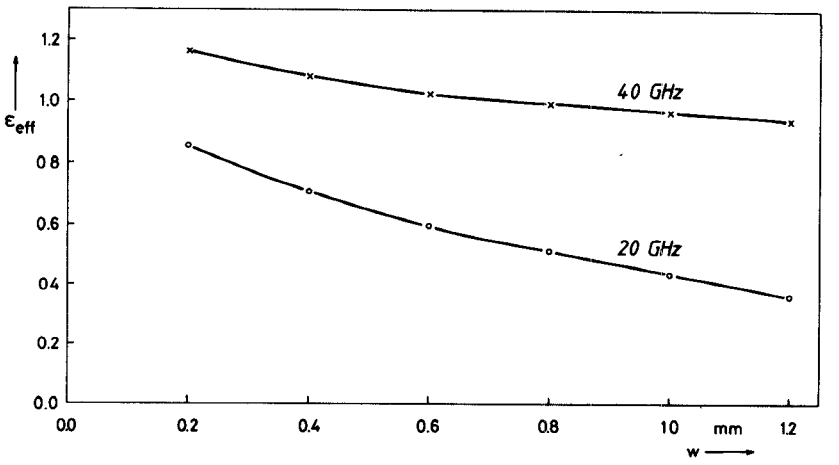

Fig. 6. Effective dielectric constant of a unilateral finline versus slot width $w = 2\cdot(s_2 - s_1)$. ×, ○ results taken from [5], —— this method, parameters: $a = 2b = 3.556$ mm, substrate thickness 0.125 mm, $\epsilon_r = 2.2$.

of seven and nine nearly give the same propagation constants.

The accuracy of the corresponding field distributions has been checked by calculating the mode-coupling coefficients for the first 10 modes of the same finline. Here, the coupling coefficient between the ith and the jth modes is defined by

$$C_{ij} = \int_{(S)} (\boldsymbol{e}_i \times \boldsymbol{h}_j^*)\, d\boldsymbol{S} \tag{15}$$

with $\boldsymbol{e}_i$ ($\boldsymbol{h}_j$) the transverse electric- (magnetic-) field vector of the ith (jth) modes and S the finline cross section. The exact C_{ij} are given by [1]

$$C_{ij} = D_i \delta_{ij} \tag{16}$$

where δ_{ij} means Kronecker delta. For normalized modes, $D_i = 1$ for propagating modes and $D_i = \pm j$ for either inductive or capacitive evanescent modes.

The calculations have been performed by using a 100-term expansion for each electric- and magnetic-field component. The results from Table II show that C_{ij} is indeed negligibly small for $i \neq j$. It can also be observed that some of the modes behave inductively, others capacitively below cutoff. An interesting difference between them is the dependence of their propagation constants with respect to slot width. As has been displayed in Fig. 4, the propagation constants squared decrease versus slot width for inductive but increase for capacitive modes. This is confirmed by the results in Table III comparing the squared propagation constants of the first 20 modes of a bilateral finline for two different slot widths. An important consequence of this behavior is the degeneracy between inductive and capacitive modes which occurs at many combinations of the parameters slot width and frequency. Care should be taken when dealing with degenerate modes in particular in the analysis of discontinuities, because these modes are no longer orthogonal [1].

The dispersion characteristics of the first two modes in a bilateral finline are shown in Fig. 5 for two different slot widths. The agreement with results taken from [17] is excellent. The same holds for the plots of the effective dielectric constant versus slot width (Fig. 6). The results to be compared with have now been taken from [5].

V. Conclusions

It has been shown that the physical reason for any coupling between the LSE and LSM parts of the hybrid field in any generalized planar guiding structure is the restriction imposed by the edge condition. This statement also holds if the metal strips show finite thickness. Because the edge condition can be fulfilled as the final step in the analysis, both partial fields can be treated separately up to this point.

The advantages of this type of decoupling have been demonstrated by applying the singular integral equation to the analysis of finlines. With an order of the characteristic matrix of just 7, the first 30 modes can be calculated with sufficient accuracy in a few seconds. This makes it possible to perform the analysis of discontinuities with reasonable effort.

Acknowledgment

The authors gratefully acknowledge Miss C. Bühst for preparing the manuscript.

References

[1] R. E. Collin, *Field Theory of Guided Waves* New York: McGraw-Hill, 1960.

[2] R. Mittra and S. W. Lee, "*Analytical Techniques in the Theory of Guided Waves*. New York: Macmillan, 1971.

[3] T. Itoh, "Spectral domain immittance approach for dispersion characteristics of shielded microstrips with tuning septums," in *Conf. Proc. 9th EuMC*, (Brighton), 1979, pp. 435–439.

[4] T. Itoh, "Spectral domain immittance approach of dispersion characteristics of generalized printed transmission lines," *IEEE Trans. Microwave Theory Tech.*, vol. MTT-28, pp. 733–736, 1980.

[5] L. P. Schmidt, T. Itoh, and H. Hofmann, "Characteristics of unilateral fin-line structures with arbitrarily located slots," *IEEE Trans. Microwave Theory Tech.*, vol. MTT-29, pp. 352–355, 1981.

[6] L. P. Schmidt, "A comprehensive analysis of quasiplanar waveguides for mm-wave applications," in *Conf. Proc. 12th EuMC*, (Helsinki), 1982, pp. 315–320.

[7] A. M. A. El Sherbiny, "Exact analysis of shielded microstrip lines and bilateral fin-lines," *IEEE Trans. Microwave Theory Tech.*, vol. MTT-29, pp. 669–679, 1981.
[8] A. M. A. El Sherbiny, "Hybrid-mode analysis of microstrip lines on anisotropic substrates," *IEEE Trans. Microwave Theory Tech.*, vol. MTT-29, pp. 1261–1266, 1981.
[9] A. M. A. El Sherbiny, "Millimeter-wave performance of shielded slot lines," *IEEE Trans. Microwave Theory Tech.*, vol. MTT-30, pp. 750–756, 1982.
[10] L. Lewin, *Advanced Theory of Waveguides*. London: Iliffe, 1951.
[11] L. Lewin, "The use of singular integral equations in the solution of waveguide problems," in *Advances of Microwaves*, vol. 1, Leo Young, Ed. New York: Academic Press, 1966.
[12] L. Lewin, *Theory of Waveguides*. London: Neurnes Butterworths, 1975.
[13] R. Mittra and T. Itoh, "A new technique for the analysis of the dispersion characteristics of microstrip lines," *IEEE Trans. Microwave Theory Tech.*, vol. MTT-19, pp. 47–56, 1971.
[14] K. C. Gupta, R. Garg, and I. J. Bahl, *Microstrip Lines and Slot Lines*. Dedham, MA: Artech, 1979.
[15] A. S. Omar and K. Schünemann, "Formulation of the singular integral equation technique for general planar transmission lines," to be published.
[16] A. G. Sveshnikow and A. N. Tikhonow, *The Theory of Functions of a Complex Variables*. Moscow: Mir, 1971.
[17] L. P. Schmidt and T. Itoh, "Spectral domain analysis of dominant and higher-order modes in fin-lines," *IEEE Trans. Microwave Theory Tech.*, vol. MTT-28, pp. 981–985, 1980.

✤

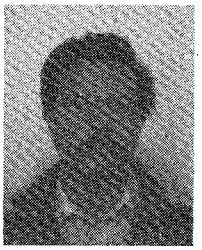

Abbas S. Omar was born in Sharkieh, Egypt, on December 9, 1954. He received the B.Sc. and M.Sc. degrees in electrical engineering from Ain Shams University, Cairo, Egypt, in 1978 and 1982, respectively.

From 1978 to 1982, he served as a Research Assistant at the Department of Electronics and Computer Engineering, Ain Shams University, Cairo, Egypt. From 1982 to 1983, he joined the Institut für Hochfrequenztechnik, Technische Universität Braunschweig, Braunschweig, West Germany, as a Research Engineer. Since then he has held the same position in the Technische Universität Hamburg-Harburg, Hamburg, West Germany. His current fields of research are the theoretical investigations of planar structures and dielectric resonators.

✤

Klaus F. Schünemann (M'76) was born in Braunschweig, Germany, on June 17, 1939. He received the Dipl. Ing. degree in electrical engineering and the Doktor-Ing. degree from Technische Universität Braunschweig, Braunschweig, Germany, in 1965 and 1970, respectively.

From 1965 to 1970, he was Assistant at the Institut für Hochfrequenztechnik of the Technische Universität Braunschweig, where he was engaged in investigations on frequency multiplication and on diode modeling for switching applications. He has published several papers on these topics. From 1970 to 1971, he was with Valvo GmbH, Hamburg, Germany, working in the area of high-power high-stable solid-state oscillators. Since 1972, he has been with the Institut für Hochfrequenztechnik of the Technische Universität Braunschweig, where he has been involved with investigations on high-speed modulators for PCM communication systems and on amplification and noise in solid-state oscillators. His current research interests are principally concerned with new technologies for microwave integrated circuits such as finline and waveguide-below-cutoff techniques.